

## 31. PETROGRAPHY OF OPAQUE MINERALS IN BASALTS DRILLED ON DSDP LEG 45

P. Eisenach, Institut für Allgemeine und Angewandte Geologie, Ludwig-Maximilians Universität, München, Federal Republic of Germany

### INTRODUCTION

Basalts have been studied for centuries, but intensive studies of the opaque mineral phases they contain, especially of the iron-titanium oxides, have only recently been undertaken. These, even if they constitute less than 1 volume per cent of the whole, are the carriers of the natural remanent magnetization (NRM). The contribution of ilmenite and sulfides to the magnetization can be neglected. Reference to the ternary system  $\text{FeO-Fe}_2\text{O}_3\text{-TiO}_2$  is necessary for interpretation of palaeomagnetism data. Different oxidation states, high temperature, deuteric oxidation (classified in six stages of increasing oxidation [Watkins, 1967]), low-temperature oxidation ( $T < 360^\circ\text{C}$ ) and, above all, doping cations—Mg, Al, and subordinate Mn—produce a wide range of mineralogic and magnetic changes. To study all these phenomena in submarine basalts, investigated so far mainly in subaerial basalts, also for submarine basalts, was the aim of this work.

Three samples of pillow basalt from Hole 395, 25 samples of coarser grained basalt and an intrusive dolerite dike from Hole 395A, and 19 samples of pillow basalt from Hole 396 were examined under reflected light. On five selected coarser grained samples, 200 microprobe analyses of iron-titanium oxides were performed to determine the different oxidation states, especially to estimate low-temperature oxidation and to specify  $f(\text{O}_2)$ -T conditions (Buddington and Lindsley, 1964) for the coexisting titanomagnetite-ilmenite phases.

In this work I attempt finally to elucidate the crystallization history and the alteration stage of the iron-titanium oxides.

### EXPERIMENTAL METHODS

Polished sections of the samples were examined in reflected light with a Leitz Ortholux Pol microscope. To aid identification of the magnetic minerals and their variable stages of maghemitization, magnetic colloids have also been used. Detailed chemical information on the iron-titanium oxides was obtained at the University of Lausanne-Dorigny, using an ARL electron probe microanalyzer.

### RESULTS

A description of each sample and the average grain sizes of opaque minerals are presented in Plates 1 through 4 and Table 1. The plates illustrate typical textures and different types of intergrowths of the opaque phases. The chemical data of the iron-titanium oxides

and the  $f(\text{O}_2)$ -T conditions, using the data of Buddington and Lindsley (1964), are listed in Table 2.

### TEXTURES

#### Hole 395

Small skeletal to anhedral grains of titanomagnetite form the bulk of opaque minerals. These grains are uniform in texture and alteration throughout the basalts. Under high magnification, one frequently can see reddish internal reflections. Larger grains show volume-change cracks, a typical sign of low-temperature oxidation.

Primary ilmenite has an elongate shape, and is occasionally mantled by titanomagnetite. Variable proportions of tiny, usually roundish grains of sulfides occur in all rocks. Microphenocrysts of porous chromium spinel occur in Samples 18-2, 31-33 cm and 18-2, 35-37 cm always show small seams of titanomagnetite. Homogeneous chromium spinels surrounded by pyroxene or plagioclase phenocrysts are not rimmed by titanomagnetite (Plate 1, Figures 1, 2).

#### Hole 395A

##### Titanomagnetite

Titanomagnetite (with a high content of  $\text{TiO}_2$ ) is present in all basalt samples. It is usually crystallized in skeletal to anhedral forms indicating a history of rapid cooling of the rocks. In the marginal zones of the pillows and at the top or at the base of thicker flows, one can see a tendency to anhedral forms, resulting from rapid cooling. In the slightly coarser grained basalts, the evolution of well-developed skeletal forms to larger subhedral forms continues. Besides the variation of grain shape and size in the more massive basalts, two size generations of titanomagnetite occur, a larger one (up to  $150\ \mu\text{m}$  grain size) with usually skeletal to subhedral forms, and a smaller one with skeletal to anhedral forms from  $10\ \mu\text{m}$  down to the limit of visibility. The smaller titanomagnetites lie near the groundmass pyroxenes, which are generally dendritic, whereas the larger titanomagnetites occur near larger phenocrysts. Observed under oil, stoichiometric titanomagnetites are a homogeneous medium brown. Grains with this appearance are very rare in these rocks, and the bulk of them show varying stages of alteration of what one presumes were original stoichiometric titanomagnetites. Reddish internal reflections, widespread mottled color, and volume-change cracks are typical signs of low-temperature oxidation in all samples—a common phenomenon of submarine basalt rocks (Petersen et al., in press; Ade-Hall and Johnson, 1976). In the volcanic

TABLE 1  
Opaque Minerals of Holes 395, 395A, and Site 396 Basalt

Sample (Interval in cm)	Lithology	Titanomagnetite	Ilmenite	Sulfides	Other Phases
11-2, 100-106	fine-grained aphy. basalt	Two generations; tiny skeletal to anhedral forms, partly as a rim round the plag.laths. The larger skeletal ones contain expansion cracks and are fringed by secondary titanomagnetite; weak anisotropic; smaller: 1 $\mu\text{m}$ -sub. larger: 50 $\mu\text{m}$ -10 $\mu\text{m}$	Small primary laths often mantled by titanomagnetite; 10-5 $\mu\text{m}$ .	Masses of small grains of pyrrhotite, especially near the iron-titanium oxides; 10 $\mu\text{m}$ -sub.	A large euhedral porous chromite
18-2, 31-33	pl.ol. phyrlic basalt	Only tiny skeletal grains (snowstars) showing reddish internal reflections under highest magnification; 10 $\mu\text{m}$ -sub.	Rare small primary laths; 10 $\mu\text{m}$ -sub.	Extremely fine roundish indet. grains; 1 $\mu\text{m}$	A large euhedral porous chromite grain, slightly mottled and rimmed by a tiny seam of titanomagnetite; 50 $\mu\text{m}$
18-2, 35-37	pl.ol.cpx. phyrlic basalt	Like Sample 18-2, 31-33 cm.			A large euhedral porous grain, partly rimmed by titanomagnetite and homogeneous ones surrounded by pyroxene and/or plag.phenocrysts; 70 $\mu\text{m}$
8-1, 127-135	aph.	Subhedral to anhedral forms; grain size down to the limit of visibility; some fringed by a fine titanomag., some showing red staining around the grains; 1 $\mu\text{m}$ -sub.	Some tiny laths and rare larger grains mantled by titanomagnetite; 10 $\mu\text{m}$ -sub.	Extremely fine grains, too small for det. 1 $\mu\text{m}$	
11-1, 56-66	aph.	Subhedral to skeletal shapes, which are contained particular in the roundish areas of the groundmass; 20 $\mu\text{m}$ -sub.	Small primary laths sometimes mantled by titanomag.; 5 $\mu\text{m}$ -sub.	Rare extremely fine indet. grains; 1 $\mu\text{m}$	
14-1, 87-99	pl.ol.ph.	Two size generations of skeletal to subhedral forms; expansion crack and mottling; partly larger ones fringed by titanomag.; tiny white reflecting particles may be hematite; larger: 60 $\mu\text{m}$ smaller: 1 $\mu\text{m}$	Increased content of small primary laths, partly arranged in a parallel direction; 30 $\mu\text{m}$	Rare small pyrrhotite and finer indet. grains; 1 $\mu\text{m}$	Rare content of iron hydroxide
14-2, 125-134	pl.ol.ph.	Two size generations of skeletal forms; larger ones displaying mottling and expansion cracks; some fringed by a sec. extra fine grained titanomag. larger: 63 $\mu\text{m}$ smaller: 5 $\mu\text{m}$	Primary laths, partly formed like titanomag. skeletons, some mantled by titanomag.; 35 $\mu\text{m}$	Rare small grains of pyrrhotite; 1 $\mu\text{m}$	Increasing content of iron hydroxide; ilmenite is partly replaced by iron hydrox. and pyrite
17-1, 46-55	pl.ol.cp.ph.	Small skeletal forms; larger displaying maghemitization and sometimes tiny fringes of hematite; 12 $\mu\text{m}$ -sub.	Usually small prim. laths; 15 $\mu\text{m}$	Small isometric pyrrhotite and pyrite; some spherical structures of original pyrite replaced by iron hydroxide	Rare large euhedral, homogeneous chromites, 10-20 $\mu\text{m}$ , show a small seam of titanomag.; seam is absent in the part lying in plag. phenocrysts; iron hydroxide in and around the displaced olivines replaces titanomag.
21-1, 112-123	pl.ol.cpx. phyrlic	Subhedral to skeletal forms; larger ones show mottling by maghemitization; 15 $\mu\text{m}$	Small prim. laths and two larger ilmeno-hematite; 20 $\mu\text{m}$	Considerable content of pyrrhotite	One large porous chromite, 60 $\mu\text{m}$ , partly rimmed by a fine seam of titanomag.; increasing content of iron hydroxide in veinlets and around the pyroxenes and olivines
22-2, 125-130	pl.ol.cpx. phyrlic	Two generations; larger one anhedral, smaller one skeletal; former are mottled; near the skeletal margins lie tiny hematite grains. Partly red-stained surrounding groundmass; larger: 12 $\mu\text{m}$ smaller: 5 $\mu\text{m}$	Larger grains, habit like titanomag. and small laths; all prim. phases; 10 $\mu\text{m}$	Small roundish pyrrhotite, partly enclosed by plag. phenocryst; 1 $\mu\text{m}$	Isometric, homogeneous chromite grain, 50 $\mu\text{m}$ , sometimes rimmed by a fine seam of titanomag.; abundant iron hydroxide, partly replacing titanomag.
23-1, 137-142	pl.ol.cpx. phyrlic	Small skeletal shapes; weak mottling and expansion cracks, some fringed by fine-grained hematite; 6 $\mu\text{m}$	Small prim. laths; 3 $\mu\text{m}$	Tiny roundish forms of indet. grains; 1 $\mu\text{m}$	Large anhedral chromite grain show a fine seam of titanomag.; 50 $\mu\text{m}$
28-1, 44-48	pl.ol. phyrlic	Small skeletal grains, altered, mottled like 23-1; 3 $\mu\text{m}$	Small prim. laths; 3 $\mu\text{m}$	Too small for det.; 1 $\mu\text{m}$	Great content of iron hydroxide, on basis of decomposition of olivine, red staining of the adjacent groundmass; euhedral chromite enclosed by plag. phenocrysts; 30 $\mu\text{m}$
31-1, 125-128	pl.ol.(cpx) phyrlic	Small skeletal grains; partly mottled by maghemitization, partly fringed by fine-grained hematite; 5 $\mu\text{m}$	Larger subhedral grains; another more common phase composed of small laths; 7 $\mu\text{m}$	Fine pyrrhotite grains surrounded by plag.ph.	Abundant content of iron hydroxide lining veinlets and vesicles; large homogeneous and porous chromites; 30 $\mu\text{m}$
32-1, 140-150	volcanic breccia	Two skeletal generations from different grain size; smaller range from 15 $\mu\text{m}$ down to the limit of visibility, larger from 150 to 30 $\mu\text{m}$ ; latter show mottling and expan. cracks. Others contain isolated coarse lamellae of ilmenite. High-temperature oxidation followed by low-temp. oxidation; larger: 130 $\mu\text{m}$ smaller: 10 $\mu\text{m}$	Prim. and secondary (lamellae) phases; former are laths, mostly mantled by titanomag., replaced by iron hydroxide again. Smaller laths displaying twin lam. and partly parallel arrangement; 60 $\mu\text{m}$	Abundant pyrrhotite and pyrite, partly as separated grains, partly as multiphase of both	Some euhedral grains of chromite; homogeneous but slight mottling; 50 $\mu\text{m}$

TABLE 1 – Continued

Sample (Interval in cm)	Lithology	Titanomagnetite	Ilmenite	Sulfides	Other Phases
33-1, 70-77	pl.ol. pyritic	Skeletal shapes of very fine grain size; expan. cracks and mottling by maghemitization; 10 $\mu$ m-sub.	Very fine prim. laths; 10 $\mu$ m-sub.	Small pyrrhotite and less pyrite; 5 $\mu$ m	Rare, homogeneous chromite grains, partly rimmed by a tiny seam of titanomag.; 15 $\mu$ m
49-1, 77-84	volcanic breccia	Two generations; smaller consists of skeletal forms (in the glassy matrix), larger are skelet. and fragments in the recrystallized areas. Expan. cracks. larger: 15 $\mu$ m smaller: 5 $\mu$ m	Relatively high content; larger show a rim of titanomag., another are small laths and show texture like titanomag. 15 $\mu$ m tabular: 40 $\mu$ m	Rare, very small indet. grains	Abundant content of iron hydroxide in or around the olivines and vesicles
52-1, 45-50	aphyric fine gr.	Extremely fine grained skeletal to anhedral forms, displaying mottling more reddish, partly colored int. reflections, and tiny rims of maghemitization 1 $\mu$ m	Tiny prim. laths and larger with seams of titanomag.	Extremely fine roundish indet. grains; 1 $\mu$ m	Iron hydroxide fills veinlets and vesicles.
57-1, 47-53	aphyric fine gr.	Very fine skeletal to anhedral shapes, yet without the reddish tints, as in 52-1; 1 $\mu$ m	Some prim. laths; 1 $\mu$ m	Rare small indet. grains; 1 $\mu$ m	
58-2, 88-94	hyaloclastit.			Some grains of pyrite enclosed by plag. phenocr., partly intergrown with pyrrhotite	
61-1, 140-150	aphyric	Small skeletal, partly fringed by extremely fine grained hematite maghemite appearances on the straits of the skeletal (for example the axes or spurs of the centers of the planes). Expan. cracks; 20 $\mu$ m-sub.	Small prim. laths, fringed likewise by hematite; 3 $\mu$ m-sub.	Some larger pyrrhotite and in the majority, small, round, ind. grains; 5 $\mu$ m	Rare iron hydroxide, mostly in vesicles
62-1, 40-50	aphyric, fine-grained	Very fine grained skeletal shapes with slight reddish tints; expan. cracks and fringes of fine hematite; 10 $\mu$ m-sub.	Many small prim. laths, some mantled by titanomag.; 5 $\mu$ m	Fine grains of pyrite and finer ones of pyrrhotite; 1 $\mu$ m	Iron hydroxide lining vesicles and replacing titanomag. under red staining of the adjacent groundmass
63-1, 0-10	pl.ol.cpx. doleritic	Two generations of skeletal forms with different grain size; smaller ones around the pyroxene boundaries; the larger ones contain a network of sec. ilmenite (lamellae) displaying hematite exsolutions to the phase boundaries of magnetite; occasional fine fringes of ilmenite around the grains. Some cracks filled by a red-brown phase (less distinct anisotropy as ilmenite); all grains show strong corrosion and numerous expan. cracks. High-temp. oxidation; larger: 150-30 $\mu$ m smaller: 15 $\mu$ m-sub.	Large prim. laths, sometimes mantled by titanomag. and secondary phase in the titanomag.; 70 $\mu$ m-sub.	Masses of small pyrite, pyrrhotite, and polyphases of these; 20 $\mu$ m	Homogeneous, euhedral chromite; 15 $\mu$ m
64-4, 115-122	pl.ol.cpx. doler.	Two generations like 63-1; larger: 150-40 $\mu$ m-sub. smaller: 5 $\mu$ m-sub.	Like 63-1; some of the grains pseudomorph. to skeletal titanomag.	Like 63-1; some spherical shapes rimmed by small magnetite grains contain pyrite-pyrrhotite intergrown. 15 $\mu$ m	Iron hydroxide fills spherical structures
64-1, 137-142	pl.ol.cpx. doler.	Two generations like 63-1; only single exsolution lamellae of ilmenite; larger: 80-30 $\mu$ m smaller: 3 $\mu$ m	Like 63-1; rare larger ones of tabular habit; 60-15 $\mu$ m		
64-2, 67-73	pl.ol.cpx. doler.	Two generations like 63-1; curiously only few grains contain single ilmenite lamellae.	Like 63-1	Content strongly decreased; rare indet. grains	Titanomag. partly replaced by iron hydroxide
64-2, 120-132	pl.ol.cpx. doler.	Very fine grained skeletal shapes show colored and a red-stained groundmass about the grains, indications of strong alteration. 3 $\mu$ m-sub.	Some small prim. laths; 5 $\mu$ m-sub.	Tiny indet. grains, 1 $\mu$ m	
64-4, 5-10	aph. fine grained	Small anhedral to skeletal forms, mostly arranged between the plag. laths of the groundmass; expan. cracks and mottling; 10 $\mu$ m-sub.	Many prim. laths contain exsolutions of hematite; 10 $\mu$ m-sub.		Some larger clusters of iron hydroxide in amygdales, usually lining veinlets and vesicles
66-2, 42-48	aph. fine-grained	Very fine grained skeletal; expan. cracks and tiny white reflecting particles near the margins; 15 $\mu$ m-sub.	Rare tiny prim. laths; 3 $\mu$ m		Like 64-4, lower content
14-6, 37-43	f. gr. ph. basalt	Very small grains show skeletal to subhedral forms, partly rimmed by a fine granulated hematite. Appear to be two types of grains with a different color and a diff. magnetic behavior. The gray-blue ones have less magnetization than the red-brown ones. The former are more oxidized (maghemite) than the other; 3 $\mu$ m	No record	Extremely fine isometric grains; no det.; 1 $\mu$ m	Rare large euhedral chromite grains, partly porous and always rimmed by a small seam of titanomag.; 140 $\mu$ m
15-1, 115-123	f. gr. pl. ph. bas.	Extremely fine grained subhedral forms; otherwise like 14-6; 2 $\mu$ m	No record	Some small grains of intergrown pyrite. Chalcopyrite sometimes replaced by iron hydroxide from margin; 1 $\mu$ m	Iron hydroxide partly replaces titanomag.; red staining of the surrounding groundmass; rare large homogeneous chromite; 43 $\mu$ m

TABLE 1 – Continued

Sample (Interval in cm)	Lithology	Titanomagnetite	Ilmenite	Sulfides	Other Phases
15-2, 8-14	f. gr. pl. ph. bas.	Finer grain size than 15-1; 2 $\mu$ m	No record	Finer than 15-1	Some euhedral microphenocrysts of dense, homogeneous chromite; 45 $\mu$ m
15-4, 72-78	f. gr. pl. ph. bas.	Very small skeletal to subhedral shapes show different stages of oxidation. Some contain expansion cracks, some fringed by fine granuled hematite. Red staining of the groundmass near the crystals; 3 $\mu$ m	Some primary laths, 2 $\mu$ m	Roundish, drop-like grains; not det.; 1 $\mu$ m	A large euhedral homogeneous chromite; content of iron hydroxide slightly increasing; 25 $\mu$ m
15-4, 53-111	f. gr. pl. px. ph. basalt	Small skeletal grains of different oxidation stages; 15 $\mu$ m-sub.	Small laths and grains of a distinct tabular habit; some are replaced by hematite from margin. 5 $\mu$ m-sub.	Small roundish indet. grains; 3 $\mu$ m	Iron hydroxide replaces titanomag., whereby the surrounding groundmass is red-stained.
16-2, 113-117	f. pl. ph. basalt	Skeletal to subhedral forms; larger ones mottled by low-temperature oxidation; 5 $\mu$ m	Rare fine primary laths; 5 $\mu$ m	Tiny grains of pyrite and pyrrhotite; 2 $\mu$ m	Larger, homogeneous euhedral chromites show fine seams of titanomag.; decreasing content of iron hydroxide; 110 $\mu$ m
16-4, 76-85	f. pl. gr. ph. bas.	Small skeletal to subhedral shapes; partly rimmed by a fine granuled hematite, partly containing expan. cracks; 5 $\mu$ m	Few small laths of primary phase; 3 $\mu$ m	No det. fine grains; 1 $\mu$ m	Chromite like 16-2; 65 $\mu$ m
18-2, 18-26	extr. f. pl. ph. basalt	Extremely fine grained; 1 $\mu$ m	Extr. fine gr.; 1 $\mu$ m		Microphenocrysts of chromite; 30 $\mu$ m
19-1, 94-102	f. gr. pl. ph. bas.	Small skeletal forms, mottled but only little expan. cracks; some fringed by fine-grained hematite; 30 $\mu$ m-sub.	Some prim. laths; 5 $\mu$ m	Fine isometric grains; 3 $\mu$ m	Large euhedral, porous chromite; 150 $\mu$ m
22-3, 95-107	f. gr. pl. px. ph. basalt	Extremely fine skeletal shapes; 1 $\mu$ m	No record	Masses of tiny grains between the plag. laths of the groundmass; 1 $\mu$ m	Large euhedral, partly porous chromite; 50 $\mu$ m
22-3, 106-117	fine gr. pl. ph. basalt	Extremely small skeletal shapes; 1 $\mu$ m	Some prim. laths; 3 $\mu$ m	Large grains enclosed by plag. phenocrysts; corrosion of pyrrhotite by pyrite produces a kind of network.	Many large euhedral chromites lie mainly near the pyrox. phenocrysts; some contain inclusions of groundmass; 70 $\mu$ m
22-3, 117-118	f. gr. pl. px. ph. bas.	Small skeletal forms; mottled and partly fringed by fine granuled hematite; 5 $\mu$ m	Rare prim. laths; 5 $\mu$ m	Tiny roundish grains; 1 $\mu$ m	A large euhedral porous chromite enclosed by pyrox.; homogeneous one lies in plag. phenocr.; 100 $\mu$ m
22-4, 77-87	f. gr. pl. ph. basalt	Extremely small skeletal forms; 1 $\mu$ m	No record	Increasing content pyrrh. ingrown with pyrite	Large euhedral chromites, partly porous, partly homogeneous, but all rimmed by a fine seam of titanomag.; 80 $\mu$ m
24-2, 87-98	f. gr. pl. ph. basalt	Few large euhedral grains and masses of small skeletal forms; some show a titanomag.-richer core; 5 $\mu$ m	Small prim. laths; 5 $\mu$ m	Very fine grain; 1 $\mu$ m	Mostly small, homogeneous and a large porous grain of chromite; increasing content of iron hyd. near the margins of pyroxenes and the decomposed spinels; 80-10 $\mu$ m
24-3, 16-24	fine gr. pl. ol. ph. basalt	Small skeletal to subhedral forms show varying oxidation stages and expan. cracks, some rimmed by hematite; 2 $\mu$ m	Rare prim. laths, some of which are mantled by titanomag.	Small pyrrh., partly enclosed by plag. phenocr.; 1 $\mu$ m	Iron hydroxide fills vesicles and cracks of pyroxene
24-3, 75-80	extr. f. gr. pl. px. phy. bas.	Extremely small skeletal forms, sometimes fringed by fine-granuled hematite; 2 $\mu$ m	No record	Tiny roundish grains and a larger grain of pyrrhotite	Large subhedral chromite with a tiny fringe of titanomag.; 150-30 $\mu$ m
25-1, 84-93	fine gr. pl. px. phy. bas.	Small euhedral to subhedral shapes, sometimes fringed by tiny sulfide grains, mottled; 10 $\mu$ m	Prim. laths; 10 $\mu$ m	Small grains and clusters of marcasite	

Note: sub = submicroscopic grain size; px. = pyroxene; phy. = phyrlic; bas = basalt; ol. = olivine; apn. = aphyric

breccia zone within phyrlic basalt (Unit P-5) and in the doleritic intrusion (Unit P-4), larger titanomagnetites occur with exsolved ilmenite lamellae (secondary ilmenite) of oxidation class 3 or 4 (Plate 1, Figures 3, 4; Plate 2, Figure 1).

Myrmekitic intergrowths of titanomagnetite with ilmenite and with the silicate groundmass (Sample 395A-32-1, 140-150 cm) demonstrate partial leaching of titanomagnetites by hydrothermal solutions (Plate 2, Figure 2).

Samples 395A-63-1, 0-10 cm shows a more distinct leaching of titanomagnetite from the crystal margin to the first exsolution lamellae of ilmenite, so that the titanomagnetite grains now are also fringed by ilmenite. The more resistant ilmenite lamellae have been left beyond the original grain borders, and now protrude into the groundmass (Plate 1, Figure 4; Plate 2, Figure 1).

### Ilmenite

Both primary and secondary ilmenite can be distinguished texturally. The former, commonly lath-shaped, occurs in all samples. In a few cases, ilmenite has a tabular habit and somewhat larger grain size. Frequently, grains are developed similar to the skeletal forms of titanomagnetite (Plate 2, Figures 3, 4, 5), making identification difficult, especially in unfavorable cross-sections. Ilmenite mantled by titanomagnetite is common. Occasionally, more altered laths contain minute lamellae of exsolved hematite. Secondary ilmenite intergrown with titanomagnetite (subsolvus exsolution lamellae) is a product of high-temperature oxidation. It occurs in Samples 395A-32-1, 140-150 cm; 395A-63-1, 0-10 cm; 395A-63-4, 115-122 cm; 395A-64-1, 137-142 cm; and 395A-64-2, 67-73 cm.

TABLE 2  
Microprobe Analyses of Iron-Titanium Oxides (wt %)

Unit	Pl. ol		Volcanic	Beginning		Dolerite	
Lithology	ph. Basalt	ph. Basalt	Breccia	of Dolerite	Dolerite		
Sample (Interval in cm)	14-1, 87-99	14-2, 125-134	32-1, 140-150	F 61-1, 140-150	63-1, 0-10	E	
Spinel Phase							
MnO	0.33	0.32	0.30	0.28	0.33	0.29	0.30
Al <sub>2</sub> O <sub>3</sub>	1.47	1.19	1.46	7.95	1.70	1.41	1.47
FeO	70.09	72.14	70.33	68.84	69.64	70.03	69.65
TiO <sub>2</sub>	23.91	23.40	23.09	19.74	21.96	21.34	21.36
MgO	0.57	0.55	0.81	0.58	0.47	0.52	0.39
Cr <sub>2</sub> O <sub>3</sub>	0.02	0.02	0.03	—	—	0.03	—
Sum	96.39	97.62	96.02	90.42	94.10	93.62	93.17
Spinel Formula							
Mn	0.011	0.011	0.010	—	0.011	0.010	0.010
Al	0.068	0.056	0.068	—	0.080	0.067	0.069
Fe <sup>2+</sup>	1.666	1.656	1.630	—	1.620	1.604	1.613
Fe <sup>3+</sup>	0.511	0.545	0.556	—	0.602	0.642	0.640
Ti	0.710	0.699	0.688	—	0.659	0.645	0.645
Mg	0.033	0.032	0.048	—	0.028	0.031	0.023
Cr	0.001	0.001	0.001	—	—	0.001	—
Recalculated Analyses							
Ilmenite Basis							
Fe <sub>2</sub> O <sub>3</sub>	36.37	38.19	37.78	—	36.93	37.83	37.34
FeO	37.36	37.78	36.34	—	36.41	35.99	36.05
Total	100.03	101.45	99.81	—	97.80	97.41	96.91
Ulvospinel Basis							
Fe <sub>2</sub> O <sub>3</sub>	20.45	22.60	22.39	—	22.31	23.62	23.12
FeO	51.69	51.81	50.18	—	49.57	48.78	48.85
Total	98.44	99.89	98.26	—	96.34	95.99	95.49
Mol% Usp.	68.4	66.1	65.2	—	64.7	62.9	63.5
S							
Rhombohedral Phase							
MnO	0.38	0.35	0.33	—	0.28	0.26	0.47
Al <sub>2</sub> O <sub>3</sub>	0.20	0.16	0.16	—	0.26	—	0.38
FeO	46.23	50.66	48.13	—	43.02	47.15	53.50
TiO <sub>2</sub>	51.13	49.13	49.86	—	49.67	48.77	41.67
MgO	0.50	0.61	0.93	—	0.40	0.32	0.69
Cr <sub>2</sub> O <sub>3</sub>	0.04	0.01	—	—	—	—	—
Sum	98.48	100.92	99.41	—	93.63	96.50	96.71
Mineral Formula							
Mn	0.008	0.007	0.007	—	0.006	0.003	0.010
Al	0.006	0.003	0.005	—	0.008	—	0.072
Fe <sup>2+</sup>	0.948	0.912	0.918	—	0.929	0.934	0.800
Fe <sup>3+</sup>	0.043	0.112	0.075	—	0.092	0.110	0.373
Ti	0.975	0.942	0.960	—	0.950	0.945	0.837
Mg	0.019	0.023	0.035	—	0.015	0.008	0.027
Cr	0.001	0.001	—	—	—	—	—
Recalculated Analyses							
Fe <sub>2</sub> O <sub>3</sub>	1.70	8.78	5.87	—	—	4.59	16.69
FeO	44.70	42.76	42.84	—	—	43.02	35.78
Total	98.65	101.80	99.99	—	—	96.96	98.68
Mol%	1.9	8.6	5.9	—	—	4.6	20.1
R <sub>2</sub> O <sub>3</sub>	810	1020	955	—	—	910	1140
Temp. (°C)	10-16.0	10-10.7	10-12.0	—	—	10-12.9	10-8.2

Note: F = fringe grain of a spherule; E = exsolved grain; S = secondary ilmenite; Recalculation procedure according to Carmichael (1967).

### Iron Hydroxides

These are abundant, but always in altered areas, veins and vesicles. They partly replace iron-titanium oxides.

### Sulfides

Sulfides make up a widespread but volumetrically subordinate mineral phase in these rocks. Pyrite and pyrrhotite are the most common sulfides, and show different shapes. Globules are abundant (a result of immiscibility of silica and sulfide melt) and are usually fringed by a fine-grained, strongly magnetic cubic phase (Plate 3, Figures 1, 2). Some of these globules contain a core of pyrite, pyrrhotite, or both; others—better characterized as spherules—contain extremely fine grained iron hydroxide which has replaced the original sulfide. A microprobe analysis of a fringe grain of such a spherule (Sample 32-1, 140-150 cm) gives a titanomagnetite with approximately 20 wt. per cent

TiO<sub>2</sub>. This titanium content is not so greatly different from that of the bulk titanomagnetites that one can demonstrate two different origins of the iron-titanium oxides. As results from Leg 34 (Ade-Hall and Johnson, 1976) illustrate, extensive analyses are necessary to resolve such problems. Only in the dolerite sample (63-1, 0-10 cm) do occasional marcasite nodules (Plate 3, Figure 3) occur. In this sample, a two-phased sulfide grain, consisting of exsolution lamellae of chalcopyrite in a pyrrhotite host, was formed.

### Chromium Spinel

This mineral is rare, and appears as isolated microphenocrysts in the rocks. Two textural varieties can be discerned: a homogeneous type and a porous type. Both kinds are normally rimmed by titanomagnetite crystals. However, when completely surrounded by pyroxene or by plagioclase phenocrysts, the homogeneous grains have no such rim.

### Hole 396

This hole cored a fairly uniform pillow basalt series. Variation in the textures of the iron-titanium oxides is correspondingly small. Mottled color, occasional volume-change cracks, and fringes of hematite indicate progressive alteration of the grains, whose last stage is typified by the diffusion of Fe into the surrounding groundmass. All these phenomena point to strong alteration during low-temperature oxidation. Ilmenite, here developed only as primary laths, is not present in all samples, and can be overlooked, because of the very small grain size (<5 μm). Roundish sulfide grains (pyrite, pyrrhotite, or a mixed phase of both) are common. In part, pyrite and pyrrhotite are intergrown with chalcopyrite, which is replaced by iron hydroxide. Chromium spinel is a microphenocryst in nearly all rocks, and is texturally similar to chromium spinels, as in Hole 395A.

### CHEMICAL ANALYSES

We analyzed pairs of coexisting titanomagnetite and primary ilmenite in five samples from three different basalt layers of Hole 395A (Table 2):

Core-Section	Interval (cm)	Piece
14-1	87-99	12
14-2	125-134	9
32-1	140-150	7
61-1	140-150	2
63-1	0-10	1

The minor elements Al and Cr show a slight preference for titanomagnetite, whereas Mg and Mn show a distinct preference for ilmenite. This is in good agreement with observations of Mathison (1976) on the Somerset Dam basic intrusion. The chemical analyses indicate significant compositional differences between primary and secondary ilmenite: Fe, Mn, Al, and Mg

prefer secondary ilmenite, and Ti prefers primary ilmenite.

Total iron, determined originally as FeO in the microprobe analyses, is expressed as FeO and Fe<sub>2</sub>O<sub>3</sub>, according to the recalculation procedure of Carmichael (1967). The temperature and oxygen fugacities corresponding to these compositions were determined from the  $f(\text{O}_2)$ -T curves of Buddington and Lindsley (1964). The average total for the spinel phase, computed on the basis of ulvospinel and ilmenite, respectively, should be close to 100 per cent, thus allowing one to check the quality of the analyses. But this check is restricted to compositions lying in the field between the ulvospinel-magnetite and the magnetite-ilmenite join. The higher the oxidation state of titanomagnetite, the greater a deviation from a total of 100 per cent should be expected. This is in good agreement with recalculated analyses of minerals seen under the petrographic microscope to be progressively more altered. Sample 395A-14-2, 125-134 cm is the least altered of all samples, and yields, from the Buddington and Lindsley curves,  $T = 1020^\circ\text{C}$  and  $f(\text{O}_2) = 10^{-10.7}\text{atm}$ —the crystallization conditions of titanomagnetite and primary ilmenite in equilibrium with each other and with the magma.

These  $f(\text{O}_2)$ -T conditions suggest that cooling of the basalt was too quick for equilibrium to develop. Opposed to this, the lower temperature and  $f(\text{O}_2)$  data from samples 395A-32-1, 140-150, 395A-63-1, 0-10, and 395A-14-1, 87-99, demonstrate a much slower cooling of basalt here, such that the iron-titanium phase was always in a state of equilibrium. Above these low temperatures, fast cooling rates prevented equilibrium. I infer high-temperature oxidation for Sample 395A-63-1, 0-10, which has a relatively hematite-rich ilmenite phase.

### Optical and Magnetic Zoning

The widespread halmyrolytic alteration of titanomagnetite in submarine basalts is of more than mere mineralogical interest. Ade-Hall and Johnson (1976) show that the cation deficiency,  $z$ , of titanomagnetite is strongly correlated with a variation of magnetic properties. One of these properties, the magnetization of the iron-titanium oxides, can be observed very well using the magnetic colloid (Plate 3, Figures 4, 5, 6; Plate 4, Figures 1, 2). Under reflected light, Sample 395A-14-2, 125-134 cm appears to have only homogeneous titanomagnetite, but the colloid test demonstrates magnetic zoning, a result of low-temperature oxidation. By contrast, in Sample 395A-61-1, 140-150 cm, there is a sharp separation between a light, nonmagnetic phase and a darker, strongly magnetic phase. Plate 4, Figure 2 shows a microprobe scan over the different magnetic areas of an oxidized titanomagnetite (titanomaghemite). The microprobe analyses of these different portions are given in Table 3. The data demonstrate a slight preference of Al, Mg, and Fe for the strongly magnetic phase, and Ti and Mn to the lighter, nonmagnetic phase. All these investigated grains are

strongly maghemitized, as the cation deficiency of the borders and the cores indicate. The cation deficiency is real, and is not a result of error in the microprobe analyses.

### SUMMARY AND DISCUSSION

In all the investigated samples, titanomagnetite is the dominant phase; ilmenite is subordinate and sulfides much less abundant. Microscopic observations show that the fine-grained, rapidly cooled basalts are characterized by fine skeletal to anhedral forms of titanomagnetite. The frequent volume-change cracks and of mottling indicate low-temperature oxidation of the rocks. This is a common appearance of titanomagnetites in submarine basalts in ocean floor basalts (Ade-Hall and Johnson, 1976; Petersen et al., in press). In contrast to subaerial basalts, high-temperature oxidation of titanomagnetite seems to be rare in ocean floor basalts, and appears to occur only in the centers of massive flows and sills (Watkins et al., 1967; Gromme et al., 1969). In good agreement with this inference, high-temperature oxidation of titanomagnetite (class 3 or 4) was found in the dolerite intrusion. Microprobe analyses of an "exsolved" titanomagnetite from the dolerite give  $f(\text{O}_2)$ -T values which are too high to represent crystallization conditions. The values of  $T = 1020^\circ\text{C}$  and  $f(\text{O}_2) = 10^{-11}\text{atm}$  obtained from Sample 395A-14-2, 125-134 cm, are similar to results from Leg 34 (Mazullo et al., 1976), and may demonstrate more typical equilibrium conditions during the crystallization of iron-titanium oxides.

The preliminary results of optical and magnetic zoning of low-temperature-oxidized titanomagnetites are similar to those of Prevot (1968).

### ACKNOWLEDGMENTS

The author wishes to acknowledge Prof. Dr. D. D. Klemm and Dr. N. Petersen for stimulating discussion during the course of this research. J. Burri provided helpful assistance in the microprobe laboratory of the University of Lausanne-Dorigny. The financial support of the Deutsche Forschungsgemeinschaft is gratefully acknowledged.

### REFERENCES

- Ade-Hall, J. M. and Johnson, H. P., 1976. Petrography of opaque minerals, Leg 34. In Hart, S. R., Yeats, R. S., et al., *Initial Reports of the Deep Sea Drilling Project*, v. 34: Washington (U.S. Government Printing Office), p. 349-362.
- Buddington, A. F. and Lindsley, D. H., 1964. Iron-titanium oxide minerals and synthetic equivalents, *J. Petrol.*, v. 5, p. 310-375.
- Carmichael, I. S. E., 1967. The iron-titanium oxides of salic volcanic rocks and their associated ferromagnesian silicates, *Contrib. Mineral. Petrol.*, v. 14, p. 36-44.
- Grommé, C. S., Wright, T. L., and Peck, D. L., 1969. Magnetic properties and oxidation of iron-titanium oxide minerals in Alae and Makaopuhi lava lakes, Hawaii, *J. Geophys. Res.*, v. 74, p. 5277-5293.
- Mathison, C. I., 1975. Magnetites and ilmenites in the Somerset Dam layered basic intrusion, southeastern Queensland, *Lithos*, v. 8, p. 93-111.

**TABLE 3**  
**Microprobe Analyses of Iron-Titanium Oxides Showing Optical and Magnetic Zoning (wt. %)**

Sample (Interval in cm)	14-2, 125-134			61-1, 140-150		61-1, 140-150		32-1, 140-150											
	1	2	3	1	2	1*	2*	1	2	3	4	5	6	7	8	9	10	11	
<b>Analysis-point</b>																			
<b>Spinel Phase</b>																			
MnO	0.31	0.30	0.30	0.35	0.36	0.30	0.30	0.30	0.26	0.27	0.30	0.28	0.26	0.31	0.32	0.28	0.29	0.31	
Al <sub>2</sub> O <sub>3</sub>	1.31	1.81	1.51	1.81	1.69	1.38	1.91	1.44	1.56	1.47	1.65	1.56	1.64	1.66	1.73	1.70	1.72	1.74	
FeO	70.92	76.60	75.91	67.32	68.79	68.03	70.41	67.56	69.97	71.77	72.62	72.37	72.63	71.93	71.37	70.01	69.15	68.85	
TiO	22.42	21.55	21.21	22.60	21.96	22.46	20.80	22.65	23.05	22.57	22.42	22.42	22.37	22.76	22.39	22.89	22.93	23.00	
MgO <sup>2</sup>	0.55	0.60	0.66	0.52	0.54	0.40	0.40	0.91	0.79	0.85	0.75	0.80	0.82	0.88	0.84	0.78	0.82	0.76	
Cr <sub>2</sub> O <sub>3</sub>	—	—	—	—	—	—	0.01	—	0.08	—	—	—	—	0.07	0.06	—	—	—	
Sum	95.51	100.86	99.59	92.60	93.34	92.56	93.83	92.86	95.70	96.93	97.74	97.43	97.72	97.60	96.72	95.66	94.90	94.66	
<b>Spinel Formula</b>																			
Mn	0.010	0.010	0.010	0.012	0.012	0.010	0.010	0.010	0.009	0.009	0.010	0.009	0.009	0.010	0.011	0.009	0.010	0.010	
Al <sub>2+</sub>	0.062	0.085	0.071	0.085	0.079	0.065	0.090	0.067	0.073	0.069	0.077	0.073	0.077	0.077	0.081	0.079	0.080	0.081	
Fe <sub>3+</sub>	1.630	1.601	1.591	1.632	1.615	1.641	1.594	1.613	1.630	1.616	1.616	1.614	1.611	1.611	1.607	1.627	1.621	1.629	
Fe	0.592	0.621	0.649	0.565	0.603	0.585	0.653	0.579	0.553	0.581	0.583	0.587	0.585	0.565	0.581	0.557	0.562	0.551	
Ti	0.673	0.647	0.640	0.675	0.659	0.675	0.628	0.677	0.686	0.675	0.670	0.670	0.669	0.678	0.668	0.682	0.679	0.684	
Mg	0.033	0.036	0.039	0.031	0.032	0.024	0.047	0.054	0.047	0.050	0.044	0.047	0.049	0.052	0.050	0.046	0.048	0.045	
Cr	—	—	—	—	—	—	—	—	0.002	—	—	—	—	0.002	0.002	—	—	—	
<b>Recalculated Analyses</b>																			
<b>Ilmenite Basis</b>																			
Fe <sub>2</sub> O <sub>3</sub>	37.88	42.46	42.42	34.82	36.43	35.46	38.06	35.64	36.87	38.69	39.22	39.13	39.32	38.63	38.38	36.97	36.36	36.01	
FeO	36.84	38.39	37.74	35.99	36.01	36.13	36.17	35.49	36.79	36.95	37.33	37.16	37.24	37.17	36.63	36.75	36.44	36.45	
Total	99.31	105.10	103.84	96.02	96.99	96.12	97.65	96.43	99.39	100.80	101.67	101.35	101.65	101.47	100.56	99.37	98.55	98.27	
<b>Ulvospinel Basis</b>																			
Fe <sub>2</sub> O <sub>3</sub>	22.94	28.11	28.28	19.73	21.80	20.51	24.20	20.55	21.52	23.65	24.28	24.19	24.42	23.46	23.47	21.72	21.08	20.69	
FeO	50.28	51.31	50.46	49.57	49.17	49.58	48.63	49.07	50.61	50.49	50.77	50.60	50.66	50.82	50.26	50.47	50.18	50.23	
Total	97.81	103.68	102.42	94.58	95.52	94.62	96.25	94.92	97.86	99.30	100.17	99.85	100.17	99.95	99.08	97.84	97.01	96.73	
Mol % Usp.	64.7	58.8	58.4	67.9	65.1	67.3	61.6	66.9	66.4	63.8	63.1	63.2	62.9	64.0	63.7	66.0	66.6	67.1	

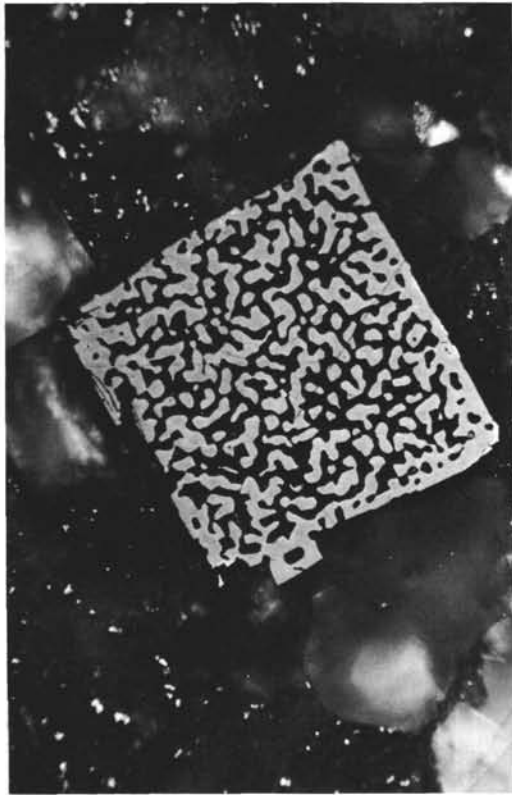
- Mazullo, L. J. and Bence, A. E., 1976. Abyssal tholeiites from DSDP Leg 34: The Nazca Plate, *J. Geophys. Res.*, v. 81, p. 4327-4351.
- Petersen N., Bleil, U. and Eisenach, P., in press. Rock- and palaeomagnetism of Leg 43 basalts. In Tucholke, B., Vogt, P., et al., *Initial Reports of the Deep Sea Drilling Project*, v. 43, Washington (U.S. Government Printing Office).
- Prévoit, M., Rémond, G. and Caye, R., 1968. Etude de la transformation d'une titanomagnétite en titanomaghémite dans une roche volcanique, *Bull. Soc. France Mineral. Cristallogr.*, v. 91, p. 65-74.
- Watkins, N. D. and Haggerty, S. E., 1967. Primary oxidation variation and petrogenesis in a single lava, *Contrib. Mineral. Petrol.*, v. 15, p. 251-271.



PLATE 1

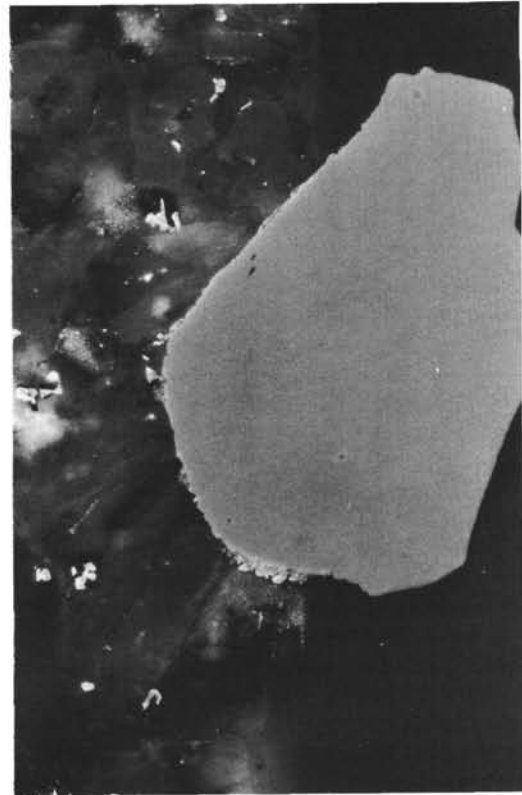
- Figure 1      Microphenocryst of a large porous chromium spinel shows limited development of a tiny seam of titanomagnetite.  
Sample 395-18-2, 35-37 cm.
- Figure 2      Microphenocryst of a large homogeneous chromium spinel, partly fringed by titanomagnetite.  
Sample 395A-17-1, 69-75 cm.
- Figure 3      Titanomagnetite of skeletal to anhedral form shows some secondary ilmenite lamellae and limited development of volume-change cracks, partly filled with sulfide phase.  
Sample 395A-63-1, 0-10 cm.
- Figure 4      High deuteric oxidation state of an exsolved titanomagnetite grain; partial leaching of titanomagnetite produces a ilmenite fringe around the grain (with colloid).  
Sample 395A-63-1, 0-10 cm.

PLATE 1



1

100 $\mu$ m



2

100 $\mu$ m



3

50 $\mu$ m



4

100 $\mu$ m

PLATE 2

- Figure 1 High oxidation state of a titanomagnetite; the more resistant ilmenite lamellae spread beyond the grain borders into the silica groundmass by progressive leaching of the titanomagnetite phase. The white reflecting phase is a pyrrhotite grain. Colloid.  
Sample 395A-63-1, 0-10 cm.
- Figure 2 Myrmekitic intergrowth of ilmenite, silica groundmass, and titanomagnetite; small relicts of titanomagnetite in the worm-shaped portions demonstrate the replacement of titanomagnetite phase by silica groundmass.  
Sample 395A-32-1, 140-150 cm.
- Figure 3 Ilmenite fringed by tiny sulfide grains formed similar to titanomagnetite skeletal; colloid shows different magnetization in the skeletal of titanomagnetite.  
Sample 395A-14-2, 125-134 cm.
- Figure 4 Ilmenite formed as skeletal titanomagnetite have been detected by magnetic colloid.  
Sample 395A-14-1, 87-99 cm.
- Figure 5 Skeletal ilmenite, formed similar to titanomagnetite skeletal, is partly mantled by titanomagnetite.  
Sample 395A-14-2, 125-134 cm.

PLATE 2



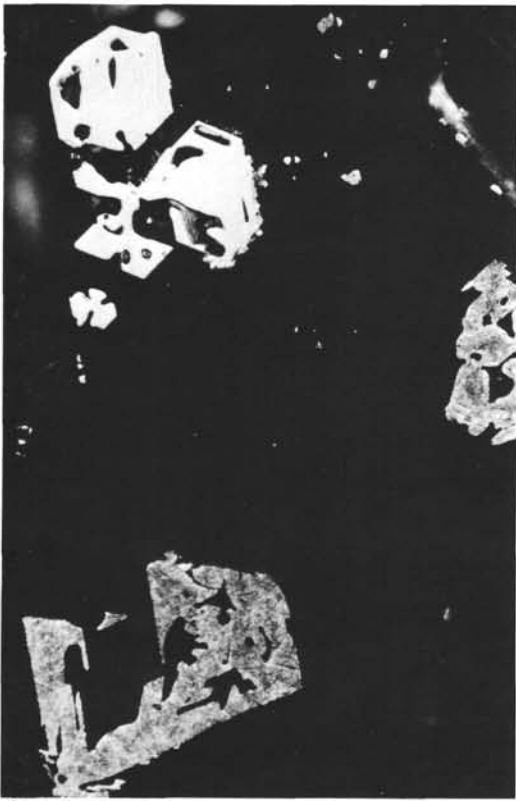
1

100μm



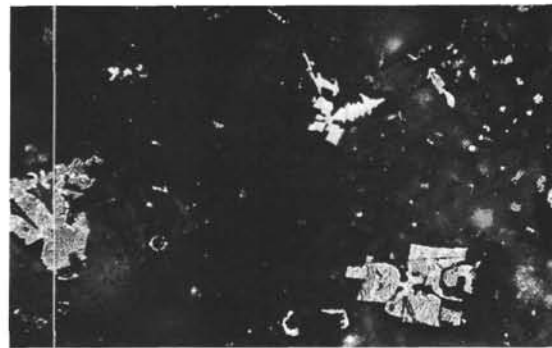
2

50μm



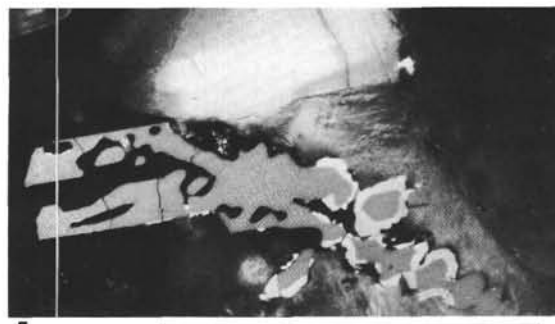
3

50μm



4

100μm



5

50μm

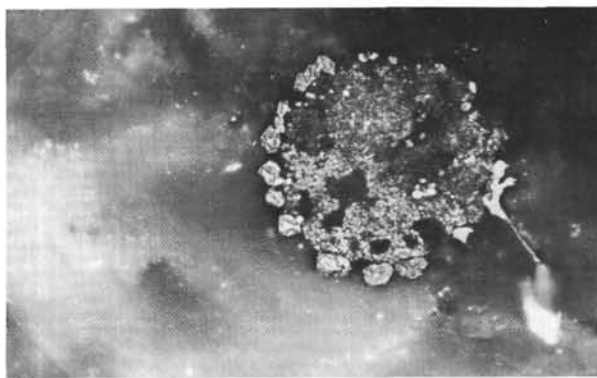
PLATE 3

- Figure 1 Small sulfide globules lie near the skeletal titanomagnetite.  
Sample 395A-14-2, 125-134 cm.
- Figure 2 Spherule of an original pyrite, now are replaced by iron hydroxide; spherule is rimmed by tiny titanomagnetite grains (see microprobe analysis, Table 2 F).  
Sample 395A-63-4, 137-142 cm.
- Figure 3 Markasite nodule, crossed nicols. Sample 395A-63-1, 0-10 cm.
- Figure 4 An optical homogeneous titanomagnetite shows magnetic zoning using the colloid test. Analyses points 1-3, see Table 3.  
Sample 395A-14-2, 125-134 cm.
- Figure 5 Shows a sharp separation into a light phase and a darker reddish brown phase.  
Sample 395A-61-1, 140-150 cm.
- Figure 6 Colloid test demonstrates the strong magnetization in the darker phase of the same grain. Analyses points 1-2, see Table 3.  
Sample 395A-61-1, 140-150 cm.

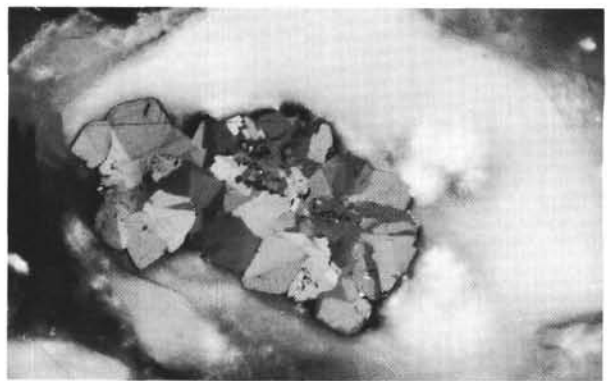
PLATE 3



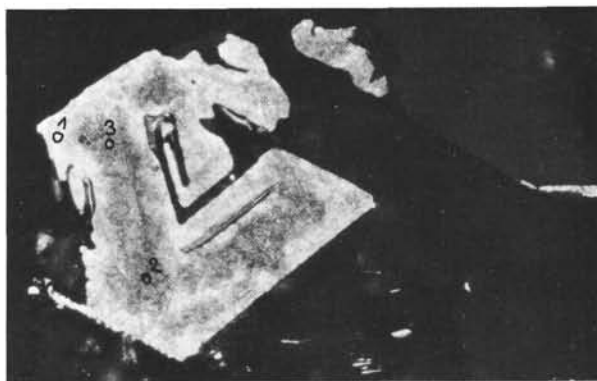
1 50 $\mu$ m



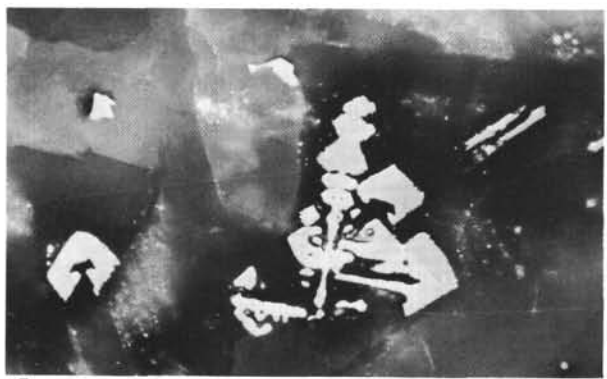
2 50 $\mu$ m



3 100 $\mu$ m



4 50 $\mu$ m



5 50 $\mu$ m



6 50 $\mu$ m

PLATE 4

- Figure 1 Colloid shows different magnetization in a skeletal titanomagnetite (snowstar). Analyses points 1\*, 2\*, see Table 3.  
Sample 395A-61-1, 140-150 cm.
- Figure 2 Colloid demonstrates magnetic zoning resulting from low-temperature oxidation. A microprobe scan (analyses points 1-11) gives the variation in the chemical composition from the more maghemitized margin to the less maghemitized and also strong magnetic core. A spherule filled by iron hydroxide is partially rimmed by tiny titanomagnetite grains.  
Sample 395A-32-1, 140-150 cm.

PLATE 4



1

50µm



2

100µm